SPARSE SIGNAL RECOVERY FOR ULTRASONIC DETECTION AND RECONSTRUCTION OF SHADOWED FLAWS

Jan Kirchhof[†], *Fabian Krieg*[†*], *Florian Römer*[†], *Alexander Ihlow*[†], *Ahmad Osman*[*], *Giovanni Del Galdo*[†**]

[†]Institute for Information Technology, Technische Universität Ilmenau, Germany
[*]Fraunhofer Institute for Nondestructive Testing IZFP, Saarbrücken, Germany
[**]Fraunhofer Institute for Integrated Circuits IIS, Ilmenau, Germany

ABSTRACT

In this paper we propose a method to improve the detection of shadowed flaws in ultrasonic non-destructive testing (NDT). The B-scans are expressed in the context of Sparse Signal Recovery (SSR), where the shadowing effect is incorporated during the reconstruction: Whenever a new defect is found, its shadow on all other dictionary atoms is determined and the dictionary is updated accordingly. We develop models for determining the affected dictionary entries as well as for the intensity of the attenuation due to the shadow. Using Orthogonal Matching Pursuit (OMP), we demonstrate that the proposed method significantly improves the reconstruction amplitudes, i.e., the detection reliability, compared to conventional detection without incorporation of shadowing.

Keywords: *Ultrasound, Non-Destructive Testing, Sparse Signal Recovery*

I. INTRODUCTION

Ultrasound is a prevalent method for Non-Destructive Testing (NDT) due to its simplicity and wide field of application [1]–[3]. The goal is to find cracks or cavities inside a specimen by recording the echoes of the ultrasonic pulse that are created by these defects due to the change in the acoustic impedance. A typical ultrasonic testing setup comprises a single ultrasound transducer that is used both as transmitter and receiver - the so-called pulse-echo mode. A single scan with this setup is called an A-scan. Several A-scans taken a long a straight line at equidistant positions can be combined to form a B-scan.

Sparse Signal Recovery (SSR) is a reconstruction technique that enables solving an underdetermined linear system of equations by finding the sparsest solution. In the context of ultrasonic (US) NDT, the measured echo signals (A-scans) can be modeled as a superposition of pulses with known shape, unknown amplitude, and unknown temporal location (delay). Therefore, their information content is comparably low, which admits a sparse representation of these signals. As a result, SSR can be applied to A-scans, which allows to achieve a temporal resolution that is superior to the one offered by the bandwidth of the measurement pulse. As shown in [4]–[6], SSR effectively deconvolves the A-scans from their pulse, leaving a train of spikes with a very high temporal resolution.

If we consider B-scans, SSR can be applied to improve the spatial and temporal resolution jointly. Due to the geometry of the pulse-echo method, isolated defects lead to hyperbola-shaped traces in every B-scan. However, the shape of the hyperbola can be distorted due to various physical effects such as dispersion of the pulse while traveling through the medium. To this end, in [7] a SSR approach based on so-called Spatial Impulse Responses (SIR) [8], [9] is proposed that can partially account for the dispersion. Alternatively, in [10], [11], it is shown how Ground Penetrating Radar (GPR) images can be decomposed using a dictionary based on parameterized hyperbolas. Since GPR and US data follow an analogous model, this approach can also be applied to ultrasonic B-scans.

All of the existing approaches consider the measurement to be a linear superposition of the echos of individual defects. Therefore, mutual influences between defects cannot be accounted for. Such influences exist, e.g., in the form of shadowing. Defects lying on a straight line with the transducer can partially block the ultrasonic energy leading to an acoustic shadow. Ignoring this effect implies a severe model mismatch which can lead to missed or spurious defects which are very undesirable in the NDT context. In [12], a simulation study was carried out to study this phenomenon and a phased array setup was proposed to avoid shadowing by adapting the insonification angle.

In this paper we show how SSR-based recovery methods can be extended to iteratively include this shadowing effect into the reconstruction process. We demonstrate our approach using the Orthogonal Matching Pursuit (OMP) algorithm.

The remainder of the paper is structured as follows: In Sec. II we introduce the signal model we use as well as the state of the art OMP SSR algorithm. In Sec. III we present the extension of the model to include shadowing and the extended OMP SSR algorithm that considers shadowing. Sec. IV presents numerical results, and Sec. V concludes the paper.

II. ALGORITHM AND DATA MODEL

II-A. Pulse-echo data model

Consider a pulse-echo setup, i.e., a single transmitter inserts an ultrasonic pulse $h(t)$ into a specimen, the pulse is reflected at one or more points in the specimen and the same transmitter receives this echo signal $y(t)$ from these reflections. For the sake of explanations, let us introduce a coordinate system with two axis, the x-axis corresponding to the different points where the A-scans are taken, and the z-axis corresponding to the direction in which the pulse is transmitted and received (cf. Figure 1). The specimen is assumed to be homogenous and isotropic with constant speed of sound c_0 and planar surface so that the z-axis corresponds with the time axis of each A-scan via $z = c_0 \cdot t$. Let $x_1^{(\mathrm{s})}, x_2^{(\mathrm{s})}, \dots x_K^{(\mathrm{s})}$ be the points where the K A-scans are taken. Then, each A-scan $y_k(t)$ can be considered as a convolution between the inserted pulse $h(t)$ and the reflectivity $s_k(t)$ of the specimen and some additional noise, i.e.,

$$y_k(t) = h(t) * s_k(t) + n_k(t). \tag{1}$$

The input pulse can be modeled as a windowed cosine-pulse of length T [13]

$$h(t) = w\left(t - \frac{T}{2}\right) \cdot \cos\left(2\pi f_c \left(t - \frac{T}{2}\right) + \phi\right), \tag{2}$$

This work was partially supported by the Carl-Zeiss Foundation under the postdoctoral scholarship project "EMBiCoS".

where f_c is the center frequency of the pulse, ϕ the phase and the window $w(t)$ is e.g., a Gaussian window of the form

$$w(t) = \begin{cases} \mathrm{e}^{-\beta t^2}, & |t| \leq \frac{T}{2} \\ 0, & \text{else,} \end{cases}$$

where the parameter β controls the width of the window.

Assuming that the pulse undergoes a discrete set of I reflections at the scattering points (x_i, z_i), the reflectivity of the k-th A-Scan $s_k(t)$ can be expressed as

$$s_k(t) = \sum_{i=1}^{I} c_i \cdot \mathrm{e}^{-\gamma \tau_k(x_i,z_i)} \cdot \delta(t - \tau_k(x_i, z_i)) \tag{3}$$

where $\delta(t)$ is the Dirac-function, c_i is the reflection coefficient, $\tau_k(x_i, z_i)$ is the time-of-flight for each reflection corresponding to the k-th A-Scan, and γ is an acoustic attenuation term that depends on the transducer and the medium (which we assume to be known). Inserting $s_k(t)$ into Eq. (1) leads to

$$y_k(t) = \sum_{i=1}^{I} c_i \cdot \mathrm{e}^{-\gamma \tau_k(x_i,z_i)} \cdot h(t - \tau_k(x_i, z_i)) + n(t). \tag{4}$$

Since processing is carried out in the digital domain, Eq. (1) is discretized in t with sampling interval t_s:

$$y_k(mt_s) = \sum_{i=1}^{I} c_i \cdot \mathrm{e}^{-\gamma \tau_k(x_i,z_i)} \cdot h(mt_s - \tau_k(x_i, z_i)) + n(mt_s).$$

Usually, the sampling frequency $f_s = \frac{1}{t_s}$ is chosen such that $f_s \gg f_c$. The samples $y_k(mt_s)$ are then stacked into a vector $\boldsymbol{y}_k = [y_k(0), y_k(t_s), \ldots, y_k((M-1)t_s)]^{\mathrm{T}} \in \mathbb{R}^M$. We repeat this procedure taking K pulse-echo scans along a straight line on the surface. The distance between those scans is given by $x_{k+1}^{(\mathrm{s})} - x_k^{(\mathrm{s})} = \delta_0$. These K scans are stacked into the overall measurement vector $\boldsymbol{y} = [\boldsymbol{y}_0, \boldsymbol{y}_1, \ldots, \boldsymbol{y}_{K-1}]^{\mathrm{T}} \in \mathbb{R}^{MK}$ representing a B-scan. Ideally, each defect leads to a trace of echos with a hyperbolic shape in $\boldsymbol{y}$. However, in practice the shape of this hyperbola is not perfectly known due to real-world effects such as dispersion of the pulse while traveling through the medium as well as the finite spatial extension of defects. To this end, we adopt a parametric description of the hyperbolas as discussed in [10], [11]

$$\tau_k(x_i, z_i, a_i) = \frac{a_i}{c_0} \cdot \sqrt{z_i^2 + \left(x_k^{(\mathrm{s})} - x_i\right)^2}, \tag{5}$$

The additional parameter a_i determines the curvature of the hyperbola.

II-B. Discrete SSR model

To recover the position of the scatterers with high accuracy, we need to fit the parameter triples (x_i, z_i, a_i) to the observed B-scan $\boldsymbol{y}$. Since all parameters are continuous, this is in general a difficult task. However, we can reformulate the problem as a discrete SSR model by introducing a grid in x, z as well as a. To this end, introduce a regular $N_x \times N_z$ discretization of the x- and z-axis within the region of interest, leading to a total number of $N = N_x \cdot N_z$ pixels with a pixel size $(\Delta x) \times (\Delta z)$ as depicted in Fig. 1. Here, each pixel represents a potential scatterer located at the pixel center. At the same time, we define a J-point discretization of the parameter a within a certain search range $[a_{\min}, a_{\max}]$.

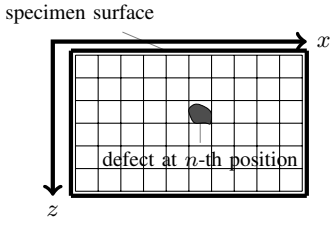

Fig. 1: SSR grid model.

Then, $\boldsymbol{y}$ can be written as a linear superposition of atoms $\boldsymbol{h}_{x,z,a} \in \mathbb{R}^{MK}$, where the elements of $\boldsymbol{h}_{x,z,a}$ are given by $\mathrm{e}^{-\gamma \tau_k(x,z,a)} \cdot h(mt_s - \tau_k(x, z, a))$ for $m = 0, 1, \ldots, M-1$ and $k = 1, 2, \ldots, K$. In other words, $\boldsymbol{h}_{x,z,a}$ contains the B-scan of a single flaw at position (x, z) with shape parameter a. Since x, z, and a have been discretized, we can write

$$\boldsymbol{y} = \boldsymbol{H}\boldsymbol{\theta} + \boldsymbol{n} \tag{6}$$

where $\boldsymbol{H} \in \mathbb{R}^{MK \times NJ}$ is the dictionary matrix containing all the vectors $\boldsymbol{h}_{x,z,a}$ as its columns, $\boldsymbol{\theta} \in \mathbb{R}^{NJ}$ contains I non-zeros corresponding to the desired scatterers and $\boldsymbol{n} \in \mathbb{R}^{MK}$ is a vector containing the noise as well as the model error. The value of each element in $\boldsymbol{\theta}$ represents the amplitude of an atom with position and scale determined by its index in $\boldsymbol{\theta}$. Since we can choose N and J and for typical choices we have $NJ \gg I$, the problem becomes sparse. The solution now is found solving the NP-hard problem

$$\min_{\boldsymbol{\theta}} \|\boldsymbol{\theta}\|_0 \text{ s. t. } \|\boldsymbol{y} - \boldsymbol{H}\boldsymbol{\theta}\|_2^2 \leq \epsilon \tag{7}$$

for each scan, where $\|\boldsymbol{\theta}\|_0 = \#(i|\theta_i \neq 0)$ is the ℓ_0-pseudo-norm that counts the number of non-zero elements of a vector and ϵ is an estimate of the noise power or approximation error. Eq. (7) is a very well studied problem that has a manifold of efficient algorithms to solve it [14], e.g., Orthogonal Matching Pursuit (OMP) [15] or Basis Pursuit Denoising (BPDN) [16]. As an example, an OMP algorithm to solve the SSR problem is shown in Algorithm 1.

Data: Dictionary $\boldsymbol{H} = [\boldsymbol{h}_1, \boldsymbol{h}_2, \cdots, \boldsymbol{h}_{NJ}]$;
Observed B-Scan vector $\boldsymbol{y}$;
$j = 1$, $s = \emptyset$;
inital residual $\boldsymbol{r} = \boldsymbol{y}$;
while $\epsilon > \epsilon_{min}$ **do**
  compute correlation: $\boldsymbol{c} = \boldsymbol{H}^{\mathrm{H}} \cdot \boldsymbol{r}$;
  find maximum, add to support of $\hat{\boldsymbol{x}}$: $i = \arg\max |c|$, $s = s \cup i$;
  compute $\hat{\boldsymbol{x}}_s$: $\hat{\boldsymbol{x}}_s = \boldsymbol{H}_s^{\dagger} \cdot \boldsymbol{y}$;
  Update residual: $\boldsymbol{r} = \boldsymbol{y} - \boldsymbol{H}_{\boldsymbol{s}} \cdot \hat{\boldsymbol{x}}_{\boldsymbol{s}}$;
  Compute epsilon: $\epsilon = \frac{\|\boldsymbol{r}\|_2}{\|\boldsymbol{y}\|_2}$;
  $j = j + 1$;
end

Algorithm 1: Orthogonal Matching Pursuit

III. INCORPORATING THE EFFECT OF SHADOWING

III-A. Shadow model

The SSR algorithms discussed in Section II implicitly assume that the observation can be modeled as a linear superposition of the responses of individual point-like scatterers. Therefore, they cannot model any interactions between different defects. However, such interactions exist in practice. Most prominently, if two defects are on one line with the transducer, the first one will reflect a significant portion of the acoustic energy, leaving the second one in shadow. Therefore, the assumed hyperbolas may have significant attenuations ("holes"), which existing SSR methods do not account for. This can lead to a significant model mismatch which may result in missed or spurious detections.

We therefore present a solution for this problem. Our proposed shadow model is a combination of a geometrical model (to determine if a dictionary atom is shadowed by another) and the results of a quantitative simulation study using CIVA [17] (to determine the mask for the shadow width and shape).

The geometrical model for determining shadows is illustrated in Fig. 2. Each defect is assumed to be circular with radius $\frac{\Delta x}{2}$. The shadow is then bounded by the lines tangent to this circle starting from the scan position (dashed black lines). To determine if another defect is inside the shadow, the intersection of the shadow

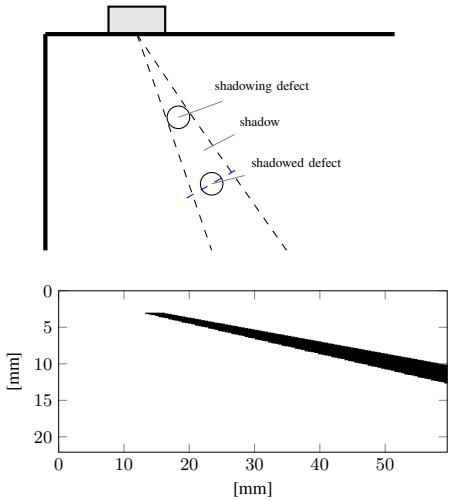

Fig. 2: Geometrical model for shadow determination and computed shadow zone.

boundaries and the circle's diameter (dashed blue auxiliary line) are computed. If $\boldsymbol{v_1}$ and $\boldsymbol{v_2}$ are the vectors pointing at these intersections and $\boldsymbol{q}$ is the vector pointing at the defect position, then this defect is inside the shadow zone bounded by the two tangents, if

$$\lambda = \frac{(\boldsymbol{v_2} - \boldsymbol{v_1})^{\mathrm{T}}(\boldsymbol{q} - \boldsymbol{v_1})}{\|\boldsymbol{v}_2 - \boldsymbol{v}_1\|_2^2} \in (0, 1). \tag{8}$$

It was observed in numerical simulations that acoustic shadows are not binary, i.e., inside the shadowing cone described by (8) the attenuation follows a smooth, gradual trend. This is due to the fact that acoustic energy can partially be diffracted around defects. Since a full physical model of this effect is very difficult and computationally demanding, we have applied a systematic quantitative study using CIVA, varying distances and radii of Side-Drilled Holes (SDH) and measuring the amount of shadowing. Fig. 3 and 4 summarize the results. In Fig. 3 an overlay of several different B-Scans is depicted. A SDH of radius 2 mm at the top of the scan casts an acoustic shadow on a second defect with varying distance of 5 mm steps. The red hyperbolic lines represent cuts through the B-scans that are shown in Fig. 4 as the solid lines. From these results, masks were derived, which are depicted as the dashed lines in Fig. 4. A good approximation of the mask is given by the parameteric model

$$m(x) = 1 - \sigma e^{-\alpha \cdot (x - x_0)^2}, \tag{9}$$

where α determines the width of the mask, $\sigma \in (0, 1)$ its amplitude and x_0 its center position. The parameters α and σ mainly depend on the distance of the defects as can be seen from Figure 4. Note that for implementational simplicity, we apply the mask along the scan direction x, neglecting the fact that to be precise, we would need to define $m(x)$ following the same hyperbolic path as depicted in Fig. 3.

III-B. Extended OMP-type reconstruction algorithm

Now that we have a model for the shadowing effect given by (8) and (9), we can take it into account in the SSR step. We demonstrate this procedure using the OMP as an example, though other SSR algorithms can be modified in similar ways.

The main idea is to incorporate the shadowing effect during the reconstruction: whenever a new defect is found, its shadow on all other dictionary atoms is determined and the dictionary is updated

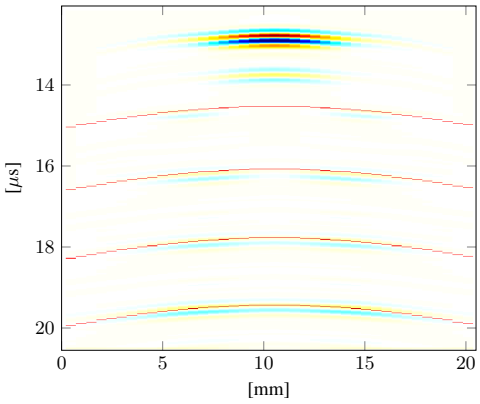

Fig. 3: Progression of the shadowing for different error distances. The red lines indicate the cuts depicted in Fig. 4.

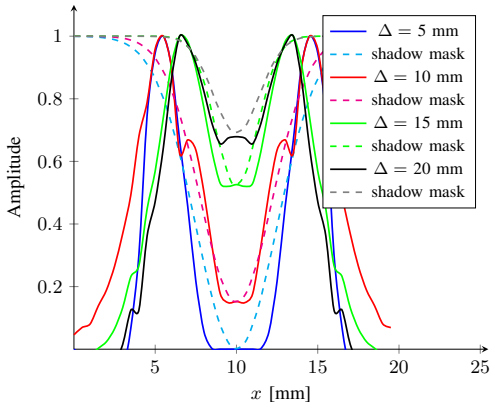

Fig. 4: Hyperbolic cuts to demonstrate the shape of the acoustic shadow depending on the distance (depicted as red lines in Fig. 3).

accordingly. Via (8) we can narrow down which atoms to update and for these we only need to compute a shadow mask according to (9). Therefore, this procedure can be implemented very efficiently. This approach implicitly assumes that the strongest, unshadowed echo will be recovered first, which is usually the case though, since the attenuation grows with the traveled distance so that the first echo is usually much stronger than subsequent ones. Moreover, since it is not shadowed it also has a better fit in the initial dictionary.

Algorithm 2 shows the enhanced version of OMP with iterative dictionary update. Modifications compared to Algorithm 1 are shown in red.

IV. RESULTS

To illustrate the potential of our new proposal, we present reconstruction results from simulation data gathered with the CIVA simulation software. A scan of a steel specimen of size $70 \times 40 \times 40$ mm^3 with $c_0 = 5900 \frac{\mathrm{m}}{\mathrm{s}}$ using a 4 MHz circular probe with 6 mm diameter is simulated with $\delta_0 = 0.5$ mm. The specimen contains two Side-Drilled Holes (SDH) with Ø= 2 mm as defects at depths of 15 and 20 mm, respectively. The lower one is inside the acoustic shadow of the upper one. For the computation of the defect response in CIVA, the separation of variables approach [18] is used.

The dictionary is set up defining a spatial grid matched to the grid of the CIVA dataset and $0.1 \leq a_j \leq 5$ with $J = 491$. The pulse $h(t)$ is chosen according to (2) where the parameters β, f_c, T are matched to the pulse observed in the measurement data

Data: Dictionary $\boldsymbol{H} = [\boldsymbol{h}_1, \boldsymbol{h}_2, \cdots, \boldsymbol{h}_N]$;
Observed B-Scan vector $\boldsymbol{y}$;
threshold ϵ_{min};
$j = 1$, $s = \emptyset$;
inital residual $\boldsymbol{r} = \boldsymbol{y}$;
while $\epsilon > \epsilon_{min}$ **do**
  compute correlation: $\boldsymbol{c} = \boldsymbol{H}^{\text{H}} \cdot \boldsymbol{r}$;
  find maximum, add to support of $\hat{\boldsymbol{x}}$: $i = \arg\max |c|$, $s = s \cup i$;
  compute $\hat{\boldsymbol{x}}_s$: $\hat{\boldsymbol{x}}_s = \boldsymbol{H}_s^{\dagger} \cdot \boldsymbol{y}$;
  Update residual: $\boldsymbol{r} = \boldsymbol{y} - \boldsymbol{H}_{\boldsymbol{s}} \cdot \hat{\boldsymbol{x}}_{\boldsymbol{s}}$;
  Compute epsilon: $\epsilon = \frac{\|\boldsymbol{r}\|_2}{\|\boldsymbol{y}\|_2}$;
  Determine list S_i of atoms that are shadowed by i;
  Update all atoms $s \in S_i$ by multiplying with mask $m(x)$ according to (9);
  $j = j + 1$;
end

Algorithm 2: OMP with iterative dictionary update.

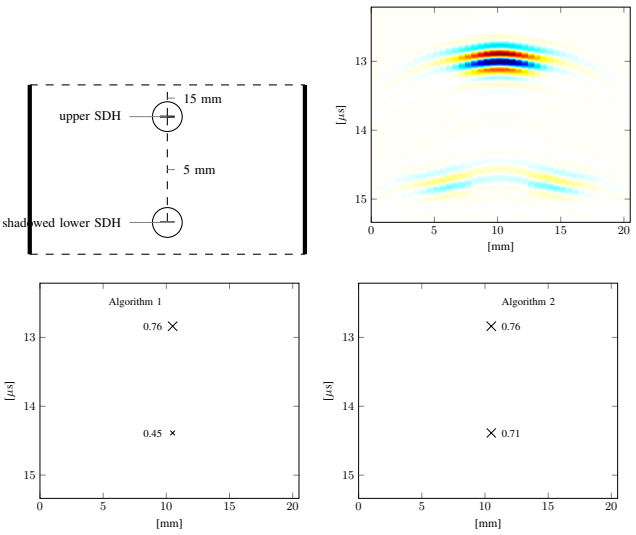

Fig. 5: Top: Sketch of the simulated specimen and simulated B-scan. Bottom: reconstructed defect positions and their respective reconstruction amplitudes using the OMP Algorithm 1 (left) and the proposed extended OMP Algorithm 2 (right), respectively.

(in response to the first SDH). This matching is obtained using numerical optimization tools, see [19] for details. Fig. 5 shows the simulated B-scan as well as the results of the reconstruction using Alg. 1 and the proposed Alg. 2, respectively. The crosses mark the reconstructed defect positions, i.e., the reconstructed (x_i, z_i), of both algorithms, whereas the amplitudes assigned to reconstructed positions are shown next to them. We observe that both algorithm detect the location accurately but the amplitude of the shadowed flaw is significantly higher in the proposed Algorithm 2.

In a second experiment, the scan of another specimen with the same parameters as the one in the above scenario was simulated. Here, two SDHs with Ø= 2 mm are varied in distance lying below a third SDH of Ø= 5 mm as sketched in Fig. 6 on the left. On the right, the three reconstructed amplitudes are plotted for varying distance between the two lower SDHs. For the OMP Algorithm 1, the amplitudes of the two lower SDHs decline with decreasing distance, since both of them move towards the shadow of the upper SDH. In contrary, the proposed extended OMP Algorithm 2 results in higher reconstructed values which leads to a better detectability of the defects. Both algorithms detect the positions correctly.

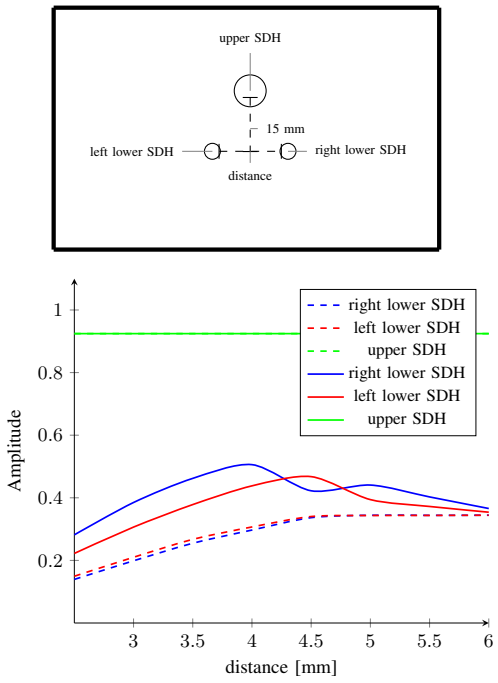

Fig. 6: Top: Sketch of the simulated specimen. Bottom: Reconstruction amplitudes of the three defects using the OMP Alg. 1 (dashed line) and the proposed extended OMP Alg. 2 (solid line). The resulting amplitudes of the proposed extended OMP Alg. 2 of the two shadowed defects are about 1.5 times the amplitudes of the OMP Alg. 1.

V. CONCLUSION

In this paper we discuss Sparse Signal Recovery (SSR)-based reconstruction methods for ultrasonic NDT. Existing methods based on SSR assume that echos from different defects superimpose linearly and hence they cannot model any mutual influence between them. Such influences exist in practice, prominently in form of shadowing of defects that lie on one line with the transducer. Ignoring this effect leads to a model mismatch that can result in missed or spurious detections. We develop a model for the intensity of the acoustic attenuation due to the shadowing effect which is based on geometrical considerations as well as extensive numerical simulations. Moreover, we introduce an iterative reconstruction algorithm based on Orthogonal Matching Pursuit that takes the shadowing into account by updating the dictionary for each detected defect. We demonstrate that the proposed algorithm significantly improves the reconstruction amplitudes, i.e., the detection reliability, compared to conventional detection without incorporation of shadowing.

VI. REFERENCES

[1] Bernd Rockstroh, Wolfgang Kappes, Friedhelm Walte, Michael Kröning, Steffen Bessert, Wolfgang Schäfer, Ralf Schallert, Werner Bähr, Dieter Joneit, Achim Montnacher, et al., "Ultrasonic and eddy-current inspection of rail wheels and wheel set axles," in *17th World Conference on Nondestructive Testing*, 2008, pp. 25–28.

[2] Wolfgang Kappes, Werner Bähr, Wolfgang Schäfer, Thomas Schwender, Andreas Knam, and Frank Knapp, "Innovative solution for ultrasonic fabrication test of railroad wheels," in *Nondestructive Evaluation/Testing (FENDT), 2014 IEEE Far East Forum on*, June 2014, pp. 340–344.

[3] Josef Krautkrämer and Herbert Krautkrämer, *Ultrasonic testing of materials*, Springer Science & Business Media, 1990.

[4] Florian Boßmann, Gerlind Plonka, Thomas Peter, Oliver Nemitz, and Till Schmitte, "Sparse deconvolution methods for ultrasonic NDT," *Journal of Nondestructive Evaluation*, vol. 31, no. 3, pp. 225–244, 2012.

[5] Christian Kexel and Jochen Moll, "Deconvolution processing for improved acoustic wavefield imaging," *Case Studies in Nondestructive Testing and Evaluation*, vol. 2, no. 0, pp. 77 – 83, 2014.

[6] Liang Wei, Zuo-ying Huang, and Pei-wen Que, "Sparse deconvolution method for improving the time-resolution of ultrasonic NDE signals," *NDT & E International*, vol. 42, no. 5, pp. 430–434, 2009.

[7] Haiteng Wu, Jian Chen, Shiwei Wu, Haoran Jin, and Keji Yang, "A model-based regularized inverse method for ultrasonic B-scan image reconstruction," *Measurement Science and Technology*, vol. 26, no. 10, pp. 105401, 2015.

[8] Bodgan Piwakowski and B Delannoy, "Method for computing spatial pulse response: Time-domain approach," *The Journal of the Acoustical Society of America*, vol. 86, no. 6, pp. 2422–2432, 1989.

[9] Bogdan Piwakowski and Khalid Sbai, "A new approach to calculate the field radiated from arbitrarily structured transducer arrays," *IEEE Transactions on Ultrasonics, Ferroelectrics, and Frequency Control*, vol. 46, no. 2, pp. 422–440, March 1999.

[10] Guillaume Terrasse, Jean-Marie Nicolas, Emmanuel Trouvé, and Émeline Drouet, "Automatic localization of gas pipes from GPR imagery," in *24th European Signal Processing Conference (EUSIPCO)*, 2016.

[11] Guillaume Terrasse, Jean-Marie Nicolas, Emmanuel Trouvé, and Émeline Drouet, "Sparse decomposition of the GPR useful signal from hyperbola dictionary," in *24th European Signal Processing Conference (EUSIPCO)*, 2016.

[12] Souad Bannouf, Sébastien Lonne, Fabrice Foucher, Jérôme Delemontez, and Laetitia Chappaz, "Simulation study to improve the detection of planar defects located under shrinkage cavities," in *11th European Conference on Non-Destructive Testing (ECNDT 2014)*, 2014.

[13] Ramazan Demirli and Jafar Saniie, "Model-based estimation of ultrasonic echoes. Part I: Analysis and algorithms," *IEEE Transactions on Ultrasonics, Ferroelectrics, and Frequency Control*, vol. 48, no. 3, pp. 787–802, May 2001.

[14] Guang-Ming Zhang, Cheng-Zhong Zhang, and David M. Harvey, "Sparse signal representation and its applications in ultrasonic NDE," *Ultrasonics*, vol. 52, no. 3, pp. 351–363, Mar. 2012.

[15] Yagyensh C. Pati, Ramin Rezaiifar, and P.S. Krishnaprasad, "Orthogonal matching pursuit: recursive function approximation with applications to wavelet decomposition," in *1993 Conference Record of The Twenty-Seventh Asilomar Conference on Signals, Systems and Computers, 1993.*, Nov 1993, pp. 40–44 vol.1.

[16] Scott Shaobing Chen, David L. Donoho, and Michael A. Saunders, "Atomic decomposition by basis pursuit," *SIAM journal on scientific computing*, vol. 20, no. 1, pp. 33–61, 1998.

[17] Extende, "CIVA NDT simulation software," 2016, http://www.extende.com/civa-in-a-few-words.

[18] M. Darmon, N. Leymarie, S. Chatillon, and S. Mahaut, *Modelling of scattering of ultrasounds by flaws for NDT*, pp. 61–71, Springer Berlin Heidelberg, 2009.

[19] Jan Kirchhof, Fabian Krieg, Florian Römer, Alexander Ihlow, Ahmad Osman, and Giovanni Del Galdo, "Speeding up 3D SAFT for ultrasonic NDT by Sparse Deconvolution," in *IEEE International Ultrasonics Symposium*, September 2016.